PERGAMON

Deep-Sea Research I 46 (1999) 1705–1731

DEEP-SEA RESEARCH
PART I

Intense nonlinear migrations of the Pacific warm pool

Doron Nof[a,b,*], Stephen Van Gorder[a]

[a]*Department of Oceanography 4320, The Florida State University, Tallahassee, FL 32306-4320, USA*
[b]*Geophysical Fluid Dynamics Institute, The Florida State University, Tallahassee, FL 32306-4320, USA*

Received 24 November 1997; received in revised form 12 January 1999; accepted 1 February 1999

Abstract

An upper bound for the nonlinear eastward propagation rate of the Pacific warm pool is derived analytically using an inertial two-and-a-half-layer model on a β plane. The model is based on the familiar idea that, in most years, the eastward migration tendency is arrested by the drag imposed on the ocean by the westward trade winds. During El Nino years, however, when the wind partially (or completely) relaxes, the pool is freed to move toward the east. The upper bound that we focus on corresponds to a rapid migration associated with a complete relaxation of the westward winds. Nonlinear analytical solutions to the above state are constructed by integrating the (inviscid) horizontal momentum equations over a control volume in a coordinate system moving steadily toward the east. A balance between the eastward flow-force (i.e., the momentum flux resulting from the eastward density gradient) and the opposing westward form-drag (exerted by the westward flowing intermediate fluid diving under the pool) is examined. It involves integrated pressure forces, integrated inertia and the integrated Coriolis forces. In the limit of a control volume with an infinitesimal north–south extent, no recirculation (i.e., no lateral exchange of mass between the fraction of the pool occupying the immediate vicinity of the equator and regions immediately to the north and south), and no cross-equatorial flows, the governing equations reduce to the equations that govern the *nonrotating* (i.e., $\beta \equiv 0$) intrusion of warm water into a resting two-layer system. This essentially means that the Coriolis force does not have any zonal component along the equator. For such conditions, the nonlinear eastward speed is found to be $[2g(\Delta\rho_1/\rho)H_1]^{1/2}\,[1-(H_2/H_1)]^{3/2}$, where $\Delta\rho_1$ is the density difference between the pool and the intermediate water underneath (i.e., the so-called intermediate layer), H_1 the undisturbed thickness of the intermediate layer ahead of the pool, and H_2 is the intermediate layer thickness under the pool. Typical values for the Pacific give a bounding propagation rate of 50–60 cm s^{-1}, which is in good agreement with the observed migration rate during both the 1982–83 El Nino and the 1997 El Nino, the only ones

* Correspondong author. Fax: + 001-904-644-2581.
E-mail address: nof@ocean.fsu.edu (D. Nof)

0967-0637/99/$ - see front matter
PII: S0967-0637(99)00024-2

in history that are known to result from an almost complete relaxation of the winds.

1. Introduction

Determination of the Pacific warm pool migration is important to our understanding of El Nino, La Nina and the Southern Oscillation. The migration is subject to strong interannual variations in phase with the Southern Oscillation Index (e.g., Picaut et al., 1996,1997). Both observations and models suggest that the eastward migration corresponds to at least a partial relaxation of the trade winds (e.g., McPhaden and Picaut, 1990; Delcroix et al., 1992; Picaut and Delcroix, 1995; Cane and Zebiak, 1985). This is in accordance with the original suggestion of Bjerknes (1969,1972), who was the first to point out that during El Nino the trade winds and the zonal oceanic sea-surface temperature gradient go through a mutual collapse.

The very first attempts to explain the eastward migration of the pool associated its movement with a simple Kelvin wave. Although the Kelvin wave speed gives the correct order of magnitude for the pool's migration, a Kelvin wave leaves the mass behind as it propagates, whereas the pool carries its mass with it. In contrast to these linear dynamics involving Kelvin waves, we shall develop here a model that includes the nonlinear terms and allows the modeled pool to carry its entire mass as it moves eastward.

The typical structure of the warm pool is shown in the top panels of Figs. 1 and 2. Although the two top panels do not correspond to the same year (and, moreover, one of them involves El Nino whereas the other does not), they do give clear top and side views of the pool. During El Nino the warm water pool ($T > 29^{\circ}$C; $\sigma_t < 22$ kg m^{-3}) is propagating toward the east because the trade winds at least partially collapse. Various numerical models, such as that of Gent and Cane (see, e.g., Murtugudde et al., 1996) and the LODYC model (Delecluse et al., 1993), have correctly reproduced the eastward movement of the pool (see, e.g., Picaut et al., 1996). To aid in the interpretation of results from complicated models of this type, and of observations, it is helpful to use analytical results based on idealized models with simplified physics and geometry.

To do so, we shall consider the model shown in Figs. 3a and b, where the top view (shown in the central panel of Fig. 3b) corresponds to a typical observational view of the top of the pool (shown in the upper panel of Fig. 1), and the side view (shown in the lower panel of Fig. 3b) corresponds to a typical observational view of the side of the pool (shown in the upper panel of Fig. 2). For simplicity, we focus on the most intense El Ninos of the century (e.g., those of 1982 and 1997), because these events correspond to an almost complete relaxation of the winds. The model consists of a warm water ($\sigma_t < 22.0$) tongue, which is usually held against the western boundary of the Pacific by the westward wind drag but is now free to move eastward. The warm water tongue overlies an ocean containing an "intermediate water" ($22 < \sigma_t < 25$), which is allowed

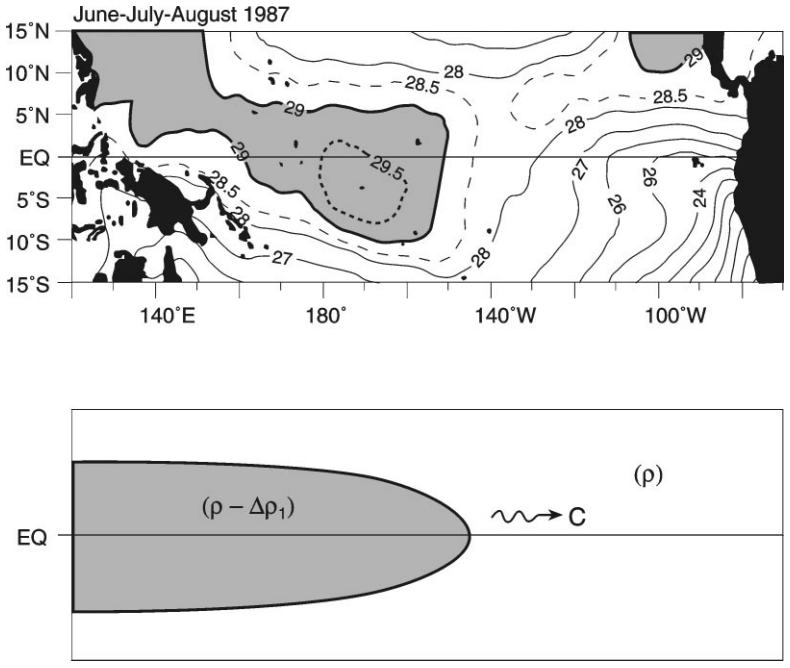

Fig. 1. *Upper panel*: Sea surface temperature (SST) in the tropical Pacific during June–July–August 1987 (El Nino). Contour interval is 1°C, except for the 28.5° and 29.5°C isotherms. SST warmer than 29°C is shaded. The western shaded region is the warm pool under discussion [reproduced from Picaut and Delcroix (1995)]. *Lower panel*: Top view of the idealized (modeled) pool; $(\rho - \Delta\rho_1)$ is the density of the pool and ρ is the density of the water ahead of and below the pool. This slightly heavier water will be referred to as "intermediate water" even though it has no relationship to what is usually called "intermediate water". The "wiggly" arrow indicates migration.

to move,[1] and an infinitely deep inactive cold lower layer ($25 < \sigma_t$). The north–south extent of the pool is a few Rossby radii (which, for a typical density anomaly of one part per thousand and a depth of 80 m, is roughly 212 km).

In our scenario, the eastward motion results from excess pressure on the western side, which is created when the winds subside. It is ultimately balanced by a form-drag exerted on the pool by the intermediate water, which, in order to compensate for the volume displaced by the eastward moving pool, is forced to dive under the pool and flow westward. In accordance with the observations that during strong El Ninos the Equatorial Undercurrent is drastically reduced (see, e.g., Firing et al., 1983; Halpern,

[1] Note that this "intermediate water" has no relationship to the much deeper water frequently referred to as "intermediate water". Furthermore, note that the intermediate water *under* the pool is sometimes referred to (by other authors) as the "barrier layer". We chose to use the term "intermediate water" rather than "barrier layer" because, in our work, the extension of the layer ahead of the pool and to the sides of the pool is exposed to the atmosphere and, consequently, does not serve as a "barrier".

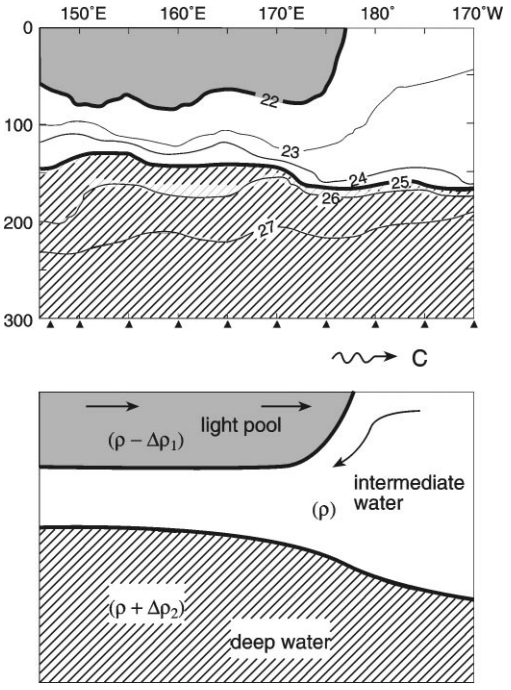

Fig. 2. *Upper panel*: Density (σ_t) along the equator in January–February 1990 (no El Nino) showing the vertical structure of the pool and the water underneath it. CTD stations are indicated by small triangles at the bottom. Contours are at intervals of 1 kg m^{-3} (density). Shading indicates densities less than 22 kg m^{-3} (the warm pool), and hatching indicates water heavier than 25 kg m^{-3} (deep water). Note that the light pool (density less than 22 kg m^{-3}) is associated with both warm water (temperature greater than 29.0°C) and low salinity ($< 35\%$) water. (Adapted from Kuroda and McPhaden, 1993.) *Lower panel*: Idealized side view of the pool. The intermediate layer separates the light pool on top from the deep water underneath; it consists of water forced to dive under the pool, (as the pool propagates eastward). Solid arrows show the velocity field (viewed from a fixed coordinate system).

1987) or even completely disappears (the 1982 El Nino), we shall neglect the motions in the deep layer ($\sigma_t > 25$).

We shall first present a scaling analysis (Section 2) illustrating that, for our strong El Nino cases, nonlinearity is important and that the local heat flux to the atmosphere is negligible when the pool's front is passing through the central Pacific. Following the scale analysis we shall present the formulation of our nonlinear two-and-a-half-layer model. The model is inviscid and nondiffusive, and is examined using a coordinate system traveling with the intrusion at (an assumed steady) speed C (Section 3). (It will become clear later that, for our detailed calculations, we shall require only an infinitesimal band of equatorial water to move steadily eastward.) Later on, in Section 4 we present the equations governing the upstream and downstream fields. This is followed by the employment of a control volume (marked by the dashed line in Fig. 3b) and an examination of the associated balance of forces. In Section 5 we show

analytically that, in the limit of very narrow control volume (i.e., $\varepsilon \to 0$), the complete β plane problem reduces to the much simpler problem of an intrusion into a two-layer system on a nonrotating plane.

This particular (theoretical) nonrotating problem has not been dealt with before, but similar problems involving laboratory experiments of gravity currents penetrating into a continuously stratified (finite-depth) ocean received much attention and are discussed in Simpson (1987). These experiments [see, e.g., Fig. 13.16 of Simpson (1987)] give a relationship between the current propagation speed and the ambient stratification. They show that the Froude number, based on the current propagation speed and the ambient stratification, is somewhere between 0.2 and 0.4. Interestingly, they display some similarity to the classical experiments of Long (1955), when the towed solid obstacle used by Long is conceptually replaced by the head of the gravity current. The analogy involves the generation of internal waves in the environmental fluid but cannot be taken much further, because the speed of Long's towed solid is given whereas the gravity current speed is determined by the field.

Given the relatively large amount of attention that these sorts of problem received from the fifties to the late seventies and early eighties, it is surprising that almost no direct progress has been made in the late eighties and nineties. Progress has been made, however, on extending existing theories (for gravity currents penetrating into a fluid with uniform density) to boundary currents on an f plane (see, e.g., Stern, 1980; Stern et al., 1982; Kubokawa and Hanawa, 1984a,b; Griffiths, 1986; Nof, 1987). These studies have shown that the presence of rotation does not arrest the migration along the wall, because it is impossible for the Coriolis force to balance the long-shore pressure gradient. The currents advance as a forever-thinning wedge, because the propagation is proportional to the thickness, which is greatest along the wall and decreases gradually as one moves away from the wall. We shall see later that similar behavior is expected to take place in the pool migration problem, where the thickness and migration rate decrease as one moves away from the equator.

Our detailed mathematical solution is presented in Section 6 and the application to the 1982 El Nino is given in Section 7. Section 8 summarizes the work.

2. Scaling

As mentioned, the basic assumption of our analysis is that, in the central Pacific, the warm pool propagates eastward in response to the wind stress going to zero. The resulting migration is due to a balance between the eastward pressure gradient (established by the eastward density gradient) and the nonlinear (advection) terms. Using scaling arguments we shall show below that this balance is valid for at least a few months. To do so, we recall that the zonal momentum equation,

$$\frac{\partial u_s}{\partial t_s} + u_s \frac{\partial u_s}{\partial x_s} + v_s \frac{\partial u_s}{\partial y_s} - \beta y_s v_s = -\frac{1}{\rho}\frac{\partial p}{\partial x_s} + \nu \frac{(1/\rho)/\partial t}{\partial z_s}, \tag{2.1}$$

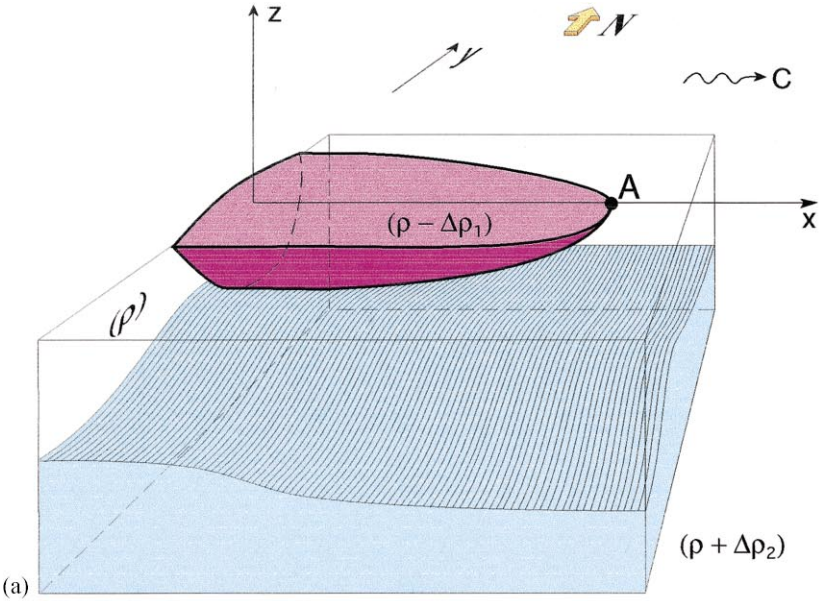

(a)

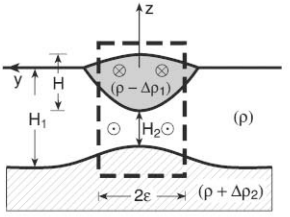

CROSS-SECTION

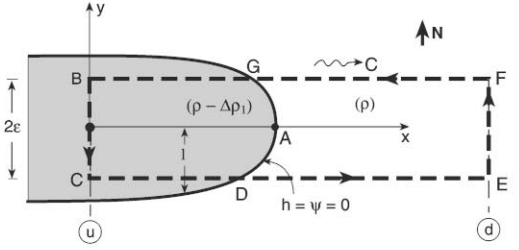

TOP VIEW

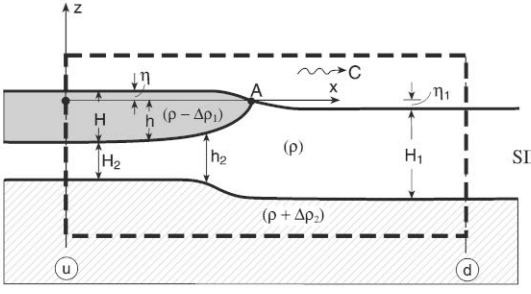

SIDE VIEW

(b)

reduces to

$$\frac{\partial u_s}{\partial t_s} + u_s \frac{\partial u_s}{\partial x_s} = -\frac{1}{\rho}\frac{\partial p}{\partial x_s} \tag{2.2}$$

in the absence of friction, wind and cross-equatorial flows (i.e., no meridional speed along the equator). Here, the notation is conventional and we view the pool from a fixed coordinate system; the subscript "s" indicates association with a stationary coordinate system (x_s, y_s, t_s). For clarity all variables are defined in both the text and Appendix A.

We also note that, in most of the existing linear models (e.g., McPhaden et al., 1988; Roemmich et al., 1994) the dominant terms are the first and last term on the left-hand side of Eq. (2.1) which are balanced by the two terms on the right-hand side of Eq. (2.1). This situation corresponds to the state where the horizontal density gradient is weak so that the pressure gradient is also weak and, consequently, can be balanced by the first or fourth term on the left-hand side of Eq. (2.1). By contrast, when the horizontal pressure gradient is as large as is frequently observed in the frontal zone of the pool [an isopycnal slope of 100 m per 20 km, according to the intersection of the $22\sigma_t$ contour with the free surface shown in Fig. 2 (reproduced from Kuroda and McPhaden (1993))], it cannot be balanced by the $\partial u_s/\partial t_s$ term in Eq. (2.2). To see this, note that, for a pool anomaly of one part per thousand, such a linear balance {i.e., $u_s \sim O[t_s g'(\partial h/\partial x_s)]$} would yield unreasonably high velocities of about $10\,\mathrm{m\,s^{-1}}$ within merely two days. Such a linear balance cannot obviously hold and, consequently, the nonlinear (second term) on the left-hand side of Eq. (2.2) becomes important and a balance between the advection and the pressure gradient is established. This balance leads to a velocity scale of $(g'h)^{1/2}$ which gives a very reasonable value of $1\,\mathrm{m\,s^{-1}}$.

It should be pointed out here that the large eastward density gradient mentioned above does not correspond directly to the wind stress that acted initially on the fluid. This is due to the nonlinear steepening that takes place during the slumping stage, i.e., from the time that the wind collapses to the final establishment of the steadily propagating state (shown in Fig. 3). This nonlinear steepening results from the fact

Fig. 3. (a) A schematic three-dimensional view of the two-and-a-half-layer model under study. The light advancing pool (red) penetrates into a two-layer ocean consisting of an intermediate upper layer (clear) and an infinitely deep lower layer (blue). Far downstream ($x \to \infty$) both the intermediate water and the deep water are at rest. To compensate for the volume displaced by the eastward moving pool, the intermediate water is forced to dive under the pool and move westward. The deep water is at rest everywhere. "A" is the "nose" of the intruding pool. (b) A cross-section of the modeled pool (top panel), a top view (central panel) and a side view of the pool (lower panel). The associated control volume is shown with the dashed line. The length of the control box is a few deformation radii, and the width is 2ε. The thicknesses H, H_1 and H_2 correspond to the pool upstream, the intermediate water downstream and the intermediate water upstream. All are taken along the equator (i.e., at $y \equiv 0$). Note that the top view (central panel) corresponds to the observations shown in Fig. 1 and the side view (lower panel) to the observed structure shown in Fig. 2. The coordinate system x, y, z is moving with the pool at speed C; the fixed coordinate system x_s, y_s, z_s is not shown.

that the local forward speed is proportional to $(g'h)^{1/2}$ (where h is the local thickness) so that particles away from the front sense a thick upper layer and move eastward faster than those close to the front (which sense a thin upper layer). In the case in question we begin with a weak initial wind-induced isopycnal slope of, say, 200 m per 10,000 km [see, e.g., Fig. 11.17 in Gill (1982)] and end up with a much steeper slope of 100 m per 20 km.

It is also worth pointing out that, within the central Pacific, the local heat loss to the atmosphere is not sufficient to "erase" the observed horizontal density gradient. To see this, recall that the change of the sea surface temperature (SST) with time is given by

$$\mathrm{d}T/\mathrm{d}t = Q/\rho C_{\mathrm{p}}h, \tag{2.3}$$

where Q is the anomalous heat flux to the atmosphere [estimated to be (on average) less than 20 W m^{-2} (Meyers et al., 1996) but can be as low as zero and as high as 80 W m^{-2}], C_{p} is the water heat capacity [4000 J/kg (°K)] and h is the warm pool's thickness (~ 50 m). For a period of, say, 90 d, Eq. (2.3) gives a horizontal temperature difference of 0.75°C corresponding to a $\Delta\rho/\rho$ of 10^{-4}, which is an order of magnitude smaller than the observed horizontal density difference [$O(10^{-3})$] considered in our model.

Finally, it should be pointed out here that the above estimates (regarding the importance of advection in the central Pacific and the smallness of the heat-flux-induced density anomalies) are consistent with the results of Picaut and Delcroix (1995), Picaut et al. (1996), Delcroix and Picaut (1998), Maes and Delecluse (1998), and Vialard and Delecluse (1998a,b). All of these studies point to the significance of advection.

3. Formulation

As an idealized formulation of the problem, consider again the situation shown in Fig. 3. The inviscid intrusion propagates eastward at the (assumed steady) propagation rate C. Downstream at $x \to +\infty$ both the intermediate and the deep fluid are at rest, but in a coordinate system traveling with the pool they appear to be moving toward the intrusion at speed $-C$. (Note that the terms "upstream" and "downstream" are used in terms of their relationship to the pool.) To compensate for the volume displaced by the advancing pool, the intermediate layer is squeezed underneath the pool and speeds up as it dives under it. The infinitely deep fluid below maintains its uniform speed $-C$, however. Mathematically, the warm-pool propagation problem is analogous to a cold-pool propagating along the bottom into a two-layer equatorial ocean (Fig. 4). This cold-pool problem is much easier to follow than the warm-pool problem and, for simplicity, we shall focus here on the cold-pool problem. After obtaining our results we shall return to the warm-pool problem (Section 7).

Using a moving coordinate system we shall connect the upstream and downstream fields without solving for the rather complicated region in between. This connection

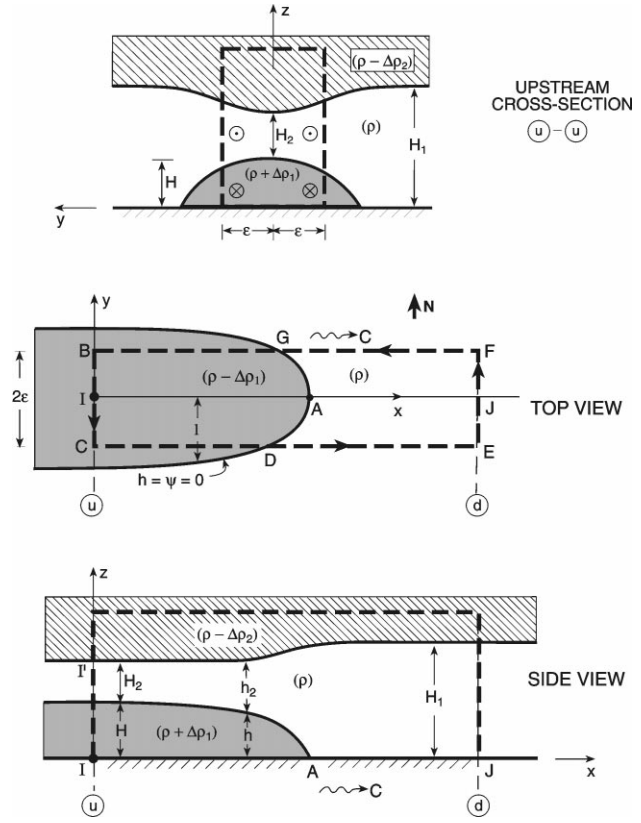

Fig. 4. A cold pool propagating along the bottom of an equatorial two-layer ocean. This situation is mathematically analogous to that shown in Fig. 3 and is considered here merely for simplicity. The origin of the fixed coordinate system (not shown) is situated upstream along the equator. The thicknesses H_1, H_2 and H are the downstream and upstream intermediate layer and cold pool thicknesses along the equator whereas h and h_2 are the pool's and the intermediate water thicknesses anywhere in the field [i.e., $H_2 = h_2(0, 0)$; $H_1 = h_2(\infty, 0)$; $H = h(0,0)$].

will be made using familiar conservation laws (e.g., potential vorticity, energy, mass) as well as the somewhat-less-familiar conservation of integrated momentum (i.e., flow-force). The latter will be obtained by integrating the x momentum equation over the (long and narrow) control volume shown in Fig. 4.

It is important to realize that when the equations of motion are transformed to a steadily moving coordinate system the original time-dependent terms in Eqs. (2.1) and (2.2) are not taken to be identically zero. Even though there are no explicit time-dependent terms in the new equations, most of the original $\partial u/\partial t$ is retained through its incorporation into the new advection terms (which comes about via the transformation $\partial/\partial t_s = -C\partial/\partial x$). The only part of the original $\partial u/\partial t$ that is not retained is the small variation relative to the moving system (i.e., $\partial/\partial t$ in the moving

system). This neglect merely implies that our results would yield the average migration speed rather than the instantaneous speed.

The fixed x_s and y_s axes are directed along and across the pool, and the system rotates at $\beta y/2$ about the vertical axis (z_s). As mentioned, the subscript "s" indicates that the variable in question is associated with a stationary coordinate system. Once we transfer the equations of motion to a moving coordinate system, we shall (in order to distinguish between the systems and keep our notation simple) use variables without any subscript. The pool thickness is denoted by h, and the "nose" of the intrusion is defined by $h = 0$ at $y = 0$.

In a similar fashion to the classical nonrotating intrusions into a single fluid (see, e.g., Von Karman, 1940; Benjamin, 1968) there is a stagnation point at the nose because a cross-section in the xz plane indicates the presence of a discontinuity in the slope of the streamline associated with the free surface ahead of the intrusion. The existence of such a stagnation point in a rotating gravity current was used by Stern et al. (1982); it is also discussed by Griffiths (1986). The reader might be interested in knowing that for nonrotating intrusions, Benjamin (1968) has elegantly shown that the discontinuity is associated with an intersection angle of 60°. The stagnation point essentially implies that the flow in the vicinity of the nose is nonhydrostatic (see, e.g., Griffiths, 1986), because the horizontal scale is not larger than the vertical. Another way to see the nonhydrostatic aspect of the problem is to recall that hydrostatic motions imply depth-independent horizontal movements (due to the two dimensionality of the horizontal pressure gradients), whereas the motions under the stagnation point are obviously depth dependent. We shall see that the implications of these nonhydrostatic motions for the flow-force balance are not severe as they extend over a very limited area [O(H) away from the nose].

For simplicity, it will be assumed that, in the immediate vicinity of the equator (i.e., within the control box) there is no recirculation in the sense that the core of the pool does not exchange mass with the surrounding fluid within the pool. This "no recirculation" assumption means that within the control box all points behind the front move eastward at the speed of the front so that there is no meridional velocity (and, consequently, no lateral exchange of either mass or momentum). In reality, there probably is some anticyclonic recirculation within the pool and such a recirculation will (geostrophically) balance some of the zonal (eastward) pressure gradient that is driving the pool eastward. This means that the recirculation would slow the pool's migration rate down so that its neglect for the purpose of computing our upper bound limit is certainly adequate. We shall return to this point in Section 7.

4. Governing equations for the upstream and downstream regions

We shall now determine the equations governing the flow several deformation radii away from the pool's leading edge (sections "u" and "d", Fig. 4). As mentioned, we shall deal with a coordinate system moving with the pool at its own speed C and assume that the water within our control box is moving steadily without changing its shape and structure with time. We shall see later that, with our method of solution,

only the intrusion in the immediate vicinity of the equator is required to move without changing its shape and structure with time, because we shall be concerned only with boxes whose north–south extent is infinitesimal. Note that the entire pool does not propagate eastward uniformly; rather, it propagates as a forever thinning tongue because the propagation rate decreases with decreasing thickness (and the thickness decreases gradually as one moves away from the equator). This implies that the maximum speed is along the equator.

The equations of motion in the moving system are obtained by using the transformations $x = x_s - Ct_s$; $y = y_s$; $t = t_s$. Downstream (i.e., ahead of the pool), in region "*d*", the speed is, by definition, identical to $-C$ everywhere, namely,

$$u = -C; \quad h_2 = H_1,$$

where h_2 is the thickness of the intermediate layer and H_1 is the undisturbed intermediate layer thickness. (Recall that the upstream and downstream fields are defined on the basis of their relationship to the pool and not the ambient flow).

Behind the nose (upstream), in region "*u*", the pool is geostrophic in the cross-stream direction (due to the presence of the equator), and has a potential vorticity $P(\psi)$ that is symmetrical relative to the equator (i.e., it is positive in the northern hemisphere and negative in the southern hemisphere) so that

$$-\partial u/\partial y + \beta y = hP(\psi) \text{ where } P(\psi) = 0 \text{ at } y = 0. \tag{4.1}$$

Here, u is the pool's horizontal velocity component in the x direction, β is the familiar variation of the Coriolis parameter with latitude and h is the pool's thickness. The deviation of the pressure in the pool from the pressure associated with a state of rest (i.e., "no pool" state) is

$$\Delta p = \Delta\rho_2 g(h_2 + h - H_1) + \Delta\rho_1\, g(h - z),$$

so that the y momentum balance for the pool upstream ($x \to 0$) is given by

$$\beta y(u + C) = -g'_2(\partial h/\partial y + \partial h_2/\partial y) - g'_1\partial h/\partial y, \tag{4.2}$$

where $g'_1 = g\,\Delta\rho_1/\rho$ and $g'_2 = g\,\Delta\rho_2/\rho$, $\Delta\rho_1$ and $\Delta\rho_2$ are the density differences between the pool and the intermediate layer and between the intermediate and upper layer (respectively), H is the upstream undisturbed thickness of the pool at $y = 0$, and it has been taken into account that the pool is one dimensional upstream. The intermediate layer is governed by the familiar potential vorticity equation and geostrophy:

$$\frac{-\partial u_2/\partial y + \beta y}{h_2} = \frac{\beta y_i}{H_1}, \tag{4.3}$$

$$\beta y(u_2 + C) = -g'_2\left(\frac{\partial h_2}{\partial y} + \frac{\partial h}{\partial y}\right), \tag{4.4}$$

where u_2 is the speed in the intermediate layer. Here, we have taken into account that (a) the upper layer fluid has originated ahead of the pool where the potential vorticity is $\beta y_i/H_1$ (where y_i is the latitude from which the parcel originated), and that (b) the excess pressure in the intermediate layer is $\Delta\rho_2 g\,(h_2 + h - H_1)$.

The upstream and downstream boundary conditions for the pool and intermediate layer are

$$h = 0 \text{ at } y = \pm\varepsilon,\ h = H \text{ at } y = 0,\ x = 0 \tag{4.5a}$$

$$h_2 = H_1 \text{ at } y \to \pm\infty, \tag{4.5b}$$

where $\pm\varepsilon$ is the north–south extent of the control volume (see Fig. 4).

5. The connection between the upstream and downstream fields

As mentioned earlier, we shall obtain the desired solution to the problem without solving for the complicated three-dimensional field near the pool's frontal leading edge. We will accomplish this by using the following connection principles.

5.1. The flow force

This is obtained by integrating the x momentum equation over the control volume shown in Fig. 4. Since the region where the motions are nonhydrostatic has a width of merely O(H), it is extremely small compared to the area of the control box and, therefore, can be neglected in the integration. The reader can convince himself (or herself) that this is correct by noting that all properties are continuous across the nonhydrostatic region. For the pool we have

$$\begin{aligned}\iint_{S_p}\left(hu\frac{\partial u}{\partial x} + vh\frac{\partial u}{\partial y}\right)\mathrm{d}x\,\mathrm{d}y - \beta\iint_{S_p} yvh\,\mathrm{d}x\,\mathrm{d}y \\ = -(g_2' + g_1')\iint_{S_p} h\frac{\partial h}{\partial x}\,\mathrm{d}x\,\mathrm{d}y - g_2'\iint_{S_p} h\frac{\partial h_2}{\partial x}\,\mathrm{d}x\,\mathrm{d}y,\end{aligned} \tag{5.1}$$

where S_p is the fractional area of the box occupied by the pool. Similarly, we have for the intermediate fluid

$$\begin{aligned}\iint_{S}\left(h_2u_2\frac{\partial h_2}{\partial x} + v_2h_2\frac{\partial u_2}{\partial y}\right)\mathrm{d}x\,\mathrm{d}y - \beta\iint_{S} yv_2h_2\,\mathrm{d}x\,\mathrm{d}y \\ = -g_2'\iint_{S} h_2\frac{\partial h_2}{\partial x}\,\mathrm{d}x\,\mathrm{d}y - g_2'\iint_{S} h_2\frac{\partial h}{\partial x}\,\mathrm{d}x\,\mathrm{d}y,\end{aligned} \tag{5.2}$$

where S is the entire area of the control box (i.e., it includes both the pool and the surrounding water). Even though v will be later neglected in accordance with our

no-recirculation (in the immediate vicinity of the equator) assumption, we have retained it in the above equations in order to demonstrate how the recirculation enters the problem.

Using the continuity equation and adding the above two equations [(5.1) and (5.2)], we find

$$\begin{aligned}
&\iint_{S_p}\left[\frac{\partial}{\partial x}(hu^2)+\frac{\partial}{\partial y}(huv)\right]\mathrm{d}x\,\mathrm{d}y-\beta\iint_{S_p} y\frac{\partial\psi}{\partial x}\,\mathrm{d}x\,\mathrm{d}y\\
&\quad+\iint_{S}\left[\frac{\partial}{\partial x}(h_2u_2^2)+\frac{\partial}{\partial y}(h_2u_2v_2)\right]\mathrm{d}x\,\mathrm{d}y-\beta\iint_{S} y\frac{\partial\psi_2}{\partial x}\,\mathrm{d}x\,\mathrm{d}y\\
&\quad=-\left(\frac{g_1'+g_2'}{2}\right)\iint_{S_p}\frac{\partial}{\partial x}(h^2)\,\mathrm{d}x\,\mathrm{d}y-\frac{g_2'}{2}\iint_{S_p} y\frac{\partial}{\partial x}(h_2+h)^2\,\mathrm{d}x\,\mathrm{d}y\\
&\quad+\frac{g_2'}{2}\iint_{S}\frac{\partial}{\partial x}(h^2)\,\mathrm{d}x\,\mathrm{d}y,
\end{aligned}\tag{5.3}$$

where ψ and ψ_2 are the conventional streamfunctions of the pool and intermediate water. (Note that the thickness h is well defined everywhere – it is positive within the pool and identically zero outside the pool.)

With the aid of Stoke's theorem, Eq. (5.3) can now be written as

$$\begin{aligned}
&-\oint_{\phi_p} hu^2\,\mathrm{d}y+\oint_{\phi_p} huv\,\mathrm{d}x+\beta\oint_{\phi_p} y\psi\,\mathrm{d}y-\oint_{\phi} h_2u_2^2\,\mathrm{d}y+\oint_{\phi} h_2u_2v_2\,\mathrm{d}x\\
&+\beta\oint_{\phi} y\psi_2\,\mathrm{d}y\\
&\quad=-\frac{g_1'}{2}\oint_{\phi_p} h^2\,\mathrm{d}y+\frac{g_2'}{2}\oint_{\phi}(h_2+h)^2\,\mathrm{d}y,
\end{aligned}\tag{5.4}$$

or

$$\begin{aligned}
&\int_C^B\left[hu^2+\frac{g_1'h^2}{2}-\beta y\psi\right]\mathrm{d}y+\int_C^B\left[hu_2^2+g_2'\frac{(h+h_2)^2}{2}-\beta y\psi_2\right]\mathrm{d}y\\
&\quad+\oint_{\phi_p} huv\,\mathrm{d}x+\oint_{\phi_p} h_2u_2v_2\,\mathrm{d}x=\int_E^F\left[H_1C^2+\frac{g_2'H_1^2}{2}-\beta y\psi_2\right]\mathrm{d}y,
\end{aligned}\tag{5.5}$$

where ψ is defined to be zero along the boundary of the pool (where $h\equiv 0$). In the limit of $\varepsilon\to 0$ (i.e., a control box with an infinitesimal width), all of the three terms involving β go to zero because they are of order ε^2. The last two terms on the left-hand side correspond to the lateral exchange of momentum. With the no-recirculation assumption they also go to zero so that Eq. (5.5) reduces to the nonrotating conservation of integrated momentum:

$$[hu^2+g_1'h^2/2+h_2u_2^2+g_2'(h+h_2)^2/2]_{x=0}=[H_1C^2+g_2'H_1^2]_{x\to\infty}.\tag{5.6}$$

5.2. Continuity

For the pool, the continuity equation gives

$$\oint_{\phi_p} hu\,\mathrm{d}y - \oint_{\phi_p} hv\,\mathrm{d}x = 0,$$

where ϕ_p is the boundary of the pool within the control box. With the no-recirculation assumption, it gives

$$\int_{-\varepsilon}^{+\varepsilon} hu\,\mathrm{d}y = 0,$$

because there is no pool downstream. We shall see later that this equation is automatically satisfied because $u = 0$ within the control box. Similarly, we have for the intermediate fluid

$$\int_{-\varepsilon}^{+\varepsilon} H_1 C\,\mathrm{d}y = \int_{-\varepsilon}^{+\varepsilon} h_2 u_2\,\mathrm{d}y. \tag{5.7}$$

5.3. Energy

Since we are seeking solutions for energy conserving flows, we may apply the Bernoulli integral along all streamlines. For hydrostatic motions in a steadily moving coordinate system, the Bernoulli invariant B is

$$(u^2 + v^2)/2 + p/\rho + gz + \beta C y^2/2 = B, \tag{5.8}$$

where p is the pressure and z is the height. Note that, in its most general form (which will be given later), the Bernoulli integral is applicable also to nonhydrostatic flows, and that all the properties are continuous within the layer. Consequently, Eq. (5.8) can be used to connect all regions where there is no significant vertical velocity, even if in between those regions the fluid goes through an area where the motions are nonhydrostatic and the vertical velocities are large. Application of Eq. (5.8) to the intermediate fluid gives

$$(y_i^2/2 - y^2/2)\beta C = (u_2^2 - C^2)/2 + g_2'(h_2 + h - H_1), \tag{5.9}$$

where, as alluded to before, the regions where we have applied Eq. (5.8) are hydrostatic because they are far from the leading edge. In the limit of $\varepsilon \to 0$ the left-hand side of Eq. (5.9) vanishes due to the symmetry of the problem relative to the equator.

5.4. Stagnation point at the nose

In addition to the constraints mentioned above, there is a constraint resulting from the condition that the nose is a double stagnation point. To see this recall that, as the relatively light ambient fluid "climbs" on top of the pool at the nose it senses

a discontinuity in the "bottom" slope implying that the speed vanishes at the equator (see, e.g., Von Karman, 1940; Benjamin, 1968; Stern et al., 1982; Griffiths, 1986). The heavy intruding fluid must also feel such a discontinuity and, therefore, it must also stagnate at the nose (see, e.g., Stern et al., 1982; Griffiths, 1986). Even though the flow near the nose is nonhydrostatic, it is possible to use the information associated with the stagnation points because the most general form of the Bernoulli invariant is not restricted to hydrostatic flows. This general form is

$$(u^2 + v^2 + w^2)/2 + p/\rho + gz + \beta C y^2/2 = B(\psi), \tag{5.10}$$

where the pressure (p) is not necessarily hydrostatic and, as before, B is a constant that varies from one streamline to another. In the limit of a narrow control box ($\varepsilon \to 0$), the last term on the left-hand side of Eq. (5.10) vanishes and the relationship reduces to the familiar Bernoulli in the nonrotating case.

5.5. The combined constraints

We shall see in the next sections that the set of constraints given in subsections (a)–(d) is sufficient for solving the problem. With the above procedure, one finds a set of five algebraic equations (integrated momentum, continuity and three energy equations) with five unknowns [U_2 (the intermediate layer speed above the pool), C, H, H_2 and p_A (the pressure at the stagnation point)] so that it is possible to obtain the desired solution to the problem.

The solution of the five equations is straightforward. The steps leading to the solution are briefly described in the next section; the reader who is interested only in the results may turn directly to Section 7.

6. Detailed solution

6.1. Equations

Consider again the cross-section of the pool along the equator shown (as the "side view") in Fig. 4. Application of the flow-force equation (5.6) gives

$$H_2 U_2^2 + \frac{g_2'}{2}[(H_2 + H)^2 - H_1^2] + g_1' \frac{H_2}{2} = H_1 C^2, \tag{6.1}$$

where the condition $u \to 0$ at $x = 0$ (i.e., no speed within the pool) has been used. Similarly, application of the continuity equation (5.7) to the intermediate fluid gives

$$-H_1 C = H_2 U_2. \tag{6.2}$$

Application of the Bernoulli principle to the intermediate fluid streamline connecting the stagnation point A to I′ (again, see the "side view" shown in Fig. 4) gives

$$\frac{p_A}{\rho} = \frac{U_2^2}{2} + \frac{g_2'}{2}(H_2 + H), \tag{6.3}$$

where p_A is the excess pressure at A (due to the intermediate layer). Similarly, application of the Bernoulli to the heavy fluid streamline connecting the stagnation point A and I gives

$$\frac{p_A}{\rho} = g'_2 H_2 + (g'_1 + g'_2)H, \tag{6.4}$$

and, finally, application of the Bernoulli to the intermediate layer along AJ gives

$$\frac{p_A}{\rho} = \frac{C^2}{2} + g'_2 H_1. \tag{6.5}$$

As already mentioned, the above five equations (6.1)–(6.5) have five unknowns U_2, C, H, H_2 and p_A and enable us to close the problem.

6.2. Solution

We first eliminate p_A/ρ between Eqs. (6.3) and (6.4),

$$U_2^2/2 = g'_1 H, \tag{6.6}$$

and then between Eqs. (6.4) and (6.5),

$$C^2/2 = g'_1 H + g'_2(H + H_2 - H_1). \tag{6.7}$$

Relation (6.7) can be easily understood in terms of a gravity waves analogy. (We shall see, shortly, however, that although this analogy between our migrating nonlinear pool and simple gravity waves can be useful, it can also be misleading).

To examine this analogy we can (temporarily) think of Eq. (6.7) as if it consists of a superposition of two waves [see the side view (lower panel) of Fig. 4]. The first is a wave on the pool's interface (i.e., the interface separating the pool and the intermediate water), and its eastward propagation is given by the first term on the right-hand side of Eq. (6.7). The second is a wave on the interface separating the intermediate and deep water above, and its propagation is given by the second term on the right-hand side of Eq. (6.7). We shall see later that $(H + H_2)$ is always smaller than H_1, implying that the second wave propagates westward. It turns out that the speed of this westward propagating wave is always slower than the speed of the first eastward propagating wave and, as a result, the entire pattern propagates *eastward*. Thus, in this simple analogy we have a combination of eastward and westward propagating waves (superimposed on each other) leading to an eastward movement, because the eastward speed is always greater than the westward speed. Recall that, as mentioned, although the analogy presented above is helpful for understanding some of the issues at hand, it is somewhat problematic because simple gravity waves do not carry mass as they propagate, whereas our nonlinear pool carries its entire mass with it as it migrates.

We now return to the derivation of the detailed solution and substitute Eq. (6.2) into Eq. (6.6) to get

$$C^2 = 2g\frac{\Delta\rho_1}{\rho}H\left(\frac{H_2}{H_1}\right)^2, \tag{6.8}$$

which can now be combined with Eq. (6.7) to give a relationship between the densities and the thicknesses,

$$\left(\frac{\Delta\rho_1}{\Delta\rho_2}\right) = \frac{H + H_2 - H_1}{H[(H_2/H_1)^2 - 1]}. \tag{6.9}$$

Leaving this relationship aside for a moment, we note that another relationship between the densities and the thicknesses can be obtained by inserting Eqs. (6.8) and (6.6) into Eq. (6.1):

$$\left(\frac{\Delta\rho_1}{\Delta\rho_2}\right) = \frac{H_1^2 - (H + H_2)^2}{4HH_2 - 4H_2^2H/H_1 + H^2}. \tag{6.10}$$

Finally, elimination of $(\Delta\rho_1/\Delta\rho_2)$ between Eqs. (6.9) and (6.10) gives a relationship between H_2 and H_1,

$$\frac{H_1^2 - (H_2 + H)^2}{4H_2 - 4H_2^2/H_1 + H} = \frac{H + H_2 - H_1}{(H_2/H_1)^2 - 1}, \tag{6.11}$$

which can also be written as,

$$\left(\frac{H + H_2 - H_1}{H_1}\right)\left[\left(\frac{H_2}{H_1}\right)^3 - \left(3 - \frac{H}{H_1}\right)\left(\frac{H_2}{H_1}\right)^2 - \frac{3H_2}{H_1} + 1\right] = 0. \tag{6.11a}$$

It gives a trivial ("no pool") solution corresponding to

$$H + H_2 - H_1 = 0 \tag{6.12}$$

[implying $\Delta\rho_1/\Delta\rho_2 \equiv 0$ by Eq. (6.9) and $C \equiv 0$ by Eq. (6.8)] and the nontrivial solution satisfying

$$(H_2/H_1)^3 - (3 - H/H_1)(H_2/H_1)^2 + 3(H_2/H_1) - 1 = 0. \tag{6.13}$$

This is a cubic equation for (H_2/H_1), which can also be written as an equation for (H/H_1):

$$H/H_1 = \frac{(1 - H_2/H_1)^3}{(H_2/H_1)^2}. \tag{6.14}$$

Using this relationship we can now obtain from Eq. (6.8) a relationship for C in terms of $\Delta\rho_1/\rho$, H_1 and H_2:

$$C = \left(2g\frac{\Delta\rho_1}{\rho}H_1\right)^{1/2}(1 - H_2/H_1)^{3/2}. \tag{6.15}$$

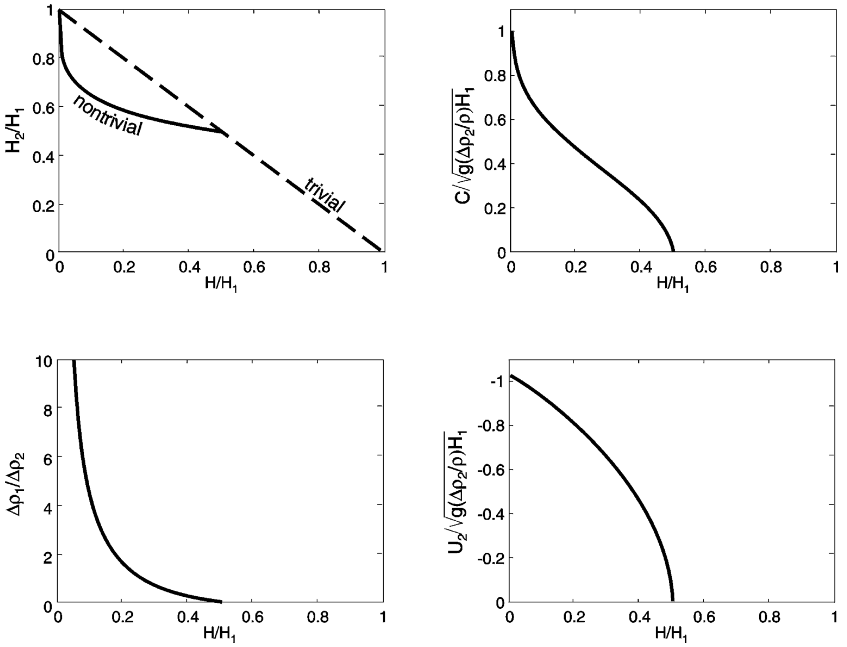

Fig. 5. The thicknesses ratio H_2/H_1 as a function of H/H_1 [i.e., the solution to Eqs. (6.12) and (6.13)] is shown in the upper left panel (which includes both the trivial and the nontrivial solution). The pool's migration speed, the density difference ratio $\Delta\rho_1/\Delta\rho_2$ and the speed above the pool as a function of the pool's thickness are shown in the upper right, lower left and lower right panels, respectively. Extension of the nontrivial solution beyond $H/H_1 = 0.5$ in the upper left panel is unphysical due to its association with a negative density difference ratio (i.e, $\Delta\rho_1/\Delta\rho_2 < 0$), which is impossible.

Eq. (6.13) has three solutions for H_2/H_1 but only one is positive (i.e., only one is physically relevant). It is shown in the upper left panel of Fig. 5. The remaining variables are shown in the upper right and lower panels of Fig. 5 and in Fig. 6. It is noteworthy that, as the lower right panel of Fig. 6 illustrates, the total thickness above the pool ($H_2 + H$) is always smaller than the upstream thickness H_1, a situation that, as we shall shortly see, is evident also in the observations. In addition, it should be pointed out that, even though there are no laboratory experiments that can be directly compared in detail to our theoretical predictions, the experiments of a gravity current entering a continuously stratified fluid of *finite depth* (see, e.g., Simpson, 1987) display speeds of the same order as our predicted values.

Before proceeding and discussing our application, it is appropriate to point out that, in the limit of $\Delta\rho_2 \to 0$ [i.e., the pool (whose density is $\rho + \Delta\rho_1$) intrudes into an infinite depth single-layer ocean with a density ρ], our results reduce to the Von Karman (1940) solution, $C = \sqrt{2g'_1 H}$, as should be the case. [Note that, as pointed out later by Benjamin (1968) and verified with our solution, the Von Karman solution does not satisfy the flow-force constraint.] In the limit of $\Delta\rho_2 \to \infty$ [i.e., the pool (whose density is, again, $\rho + \Delta\rho_1$) intrudes into a finite depth single-layer ocean with a density ρ and a depth $H_1 = H + H_2$], our results give $H/H_1 = H_2/H_1 = 0.5$,

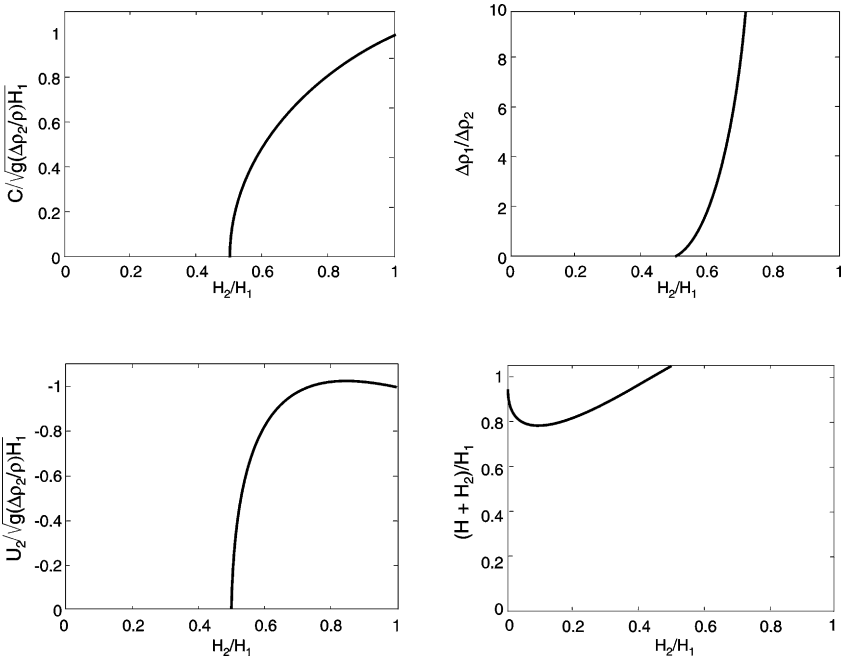

Fig. 6. The pool nondimensional migration speed $[C/(g\,\Delta\rho_2/\rho H_1)^{1/2}]$, the density difference ratio $\Delta\rho_1/\Delta\rho_2$ and the speed above the pool $[U_2/(g\,\Delta\rho_2/\rho H_1)^{1/2}]$ as a function of the nondimensional thickness above the cold pool H_2/H_1 (upper left, upper right, lower left). The total nondimensional thickness above the cold pool $(H + H_2)/H_1$ as a function of the nondimensional depth pool H/H_1 is shown in the lower right panel. Note that the total thickness above the pool, $H + H_2$, is always smaller than the upstream thickness H_1. We shall see later that this is in clear agreement with the observations.

$C = (1/2)\sqrt{2g'_1 H}$ and $U_2 = \sqrt{2g'_1 H}$, which, as required, are identical to Benjamin's (1968) results for a gravity current intruding into a finite depth fluid.

7. Application and discussion

In this section we shall compare the observed migration of the warm pool during the 1982 El Nino (the most intense El Nino of the century for which most of the data have been analyzed) to our theoretically predicted values. We chose to focus on this El Nino because, together with the 1997 El Nino (which has not been analyzed in detail yet), it is the only known event associated with an almost *complete* relaxation of the trade winds.

7.1. The chosen numerical values

We shall base our choices for the densities and thicknesses on Kuroda and McPhaden's (1993) analysis for the 1990 El Nino. Ideally, one should, of course, use

values for the 1982 El Nino rather than 1990, when there was no El Nino, but, unfortunately, for 1982 there are no measurements (of the pool) comparable in detail to those reported by Kuroda and McPhaden (1993). However, even though there was no El Nino in 1990, the warm pool did advance eastward during the observed period (Picaut et al., 1996) as required by our model. In view of this, we shall use the 1990 values and consider them to be reasonable.

To apply our model we need to choose the observational values of only *three* parameters; we shall use $\Delta\rho_1$, H_1 and H_2 because these are the three parameters that appear explicitly in our migration formula (6.15). Note that the numerical choices for these variables need to be made with care in the sense that, for consistency, we can choose only those values that lie within the validity regime of our model. Our choices [based on the observed maximum density gradient for the lower interface and a fairly arbitrary choice for the upper interface (see shaded and hatched regions in Fig. 2)] are,

$$\rho_{\text{pool}} \approx 1.022 \text{ g cm}^{-3}; \quad \rho_{\text{intermed}} \approx 1.023 \text{ g cm}^{-3}, \quad H_1 \approx 150 \text{ m}; \quad H_2 \approx 80 \text{ m}.$$

7.2. The computed values

With our solution (6.14), (6.9), (6.6) and (6.15), the chosen numerical values give a pool thickness H of about 55 m, a density difference $\Delta\rho_2$ of 0.0026 g/cm^3, a speed under pool U_2 of -1.05 m s^{-1}, and a migration rate C of 0.55 m s^{-1} (or 48 km d^{-1}). (Recall that all of the results previously described for a cold pool on the bottom are equally applicable to a warm pool on top.) All of these values are very reasonable. For clarity, we show in Fig. 7 the predicted maximum migration speed C, the observed speed, and the speed predicted by hypothetical drifters released in the numerical model of Gent and Cane (see, e.g., Murtugudde et al., 1996; Picaut et al., 1996) and in the earlier linear model (Cane and Patton, 1984). The migration speed of the pool in the Gent and Cane model is very close to that of the linear model; both are about 40% lower than our analytically predicted upper bound and 15% or so lower than the observed speed.

The difference between our model and the linear model is clear; the linear model does not contain advection of momentum so that much of our dynamics is not included in it. Consequently, the fact that our analytical prediction for the 1982 El Nino is not that different from the linear prediction is fortuitous. The difference between our model and the Gent and Cane model is less clear than the difference discussed above because the Gent and Cane model does include advection of momentum. It is probably due to the absence of friction (in our model), which is expected to increase the form-drag exerted (on the pool) and slow the pool down. Other possibilities are the neglect of motions in the lower layer and the neglect of recirculation.

7.3. The model sensitivity

To examine the sensitivity of our model to our chosen variables, we now choose three new values for $\Delta\rho_1$, H_1 and H_2. We take $\rho_{\text{pool}} \approx 1.0220$ g cm^{-3}; $\rho_{\text{intermed}} \approx 1.0235$ g cm^{-3} and new depths, $H_1 \approx 140$ m; $H_2 \approx 75$ m, instead of the previously

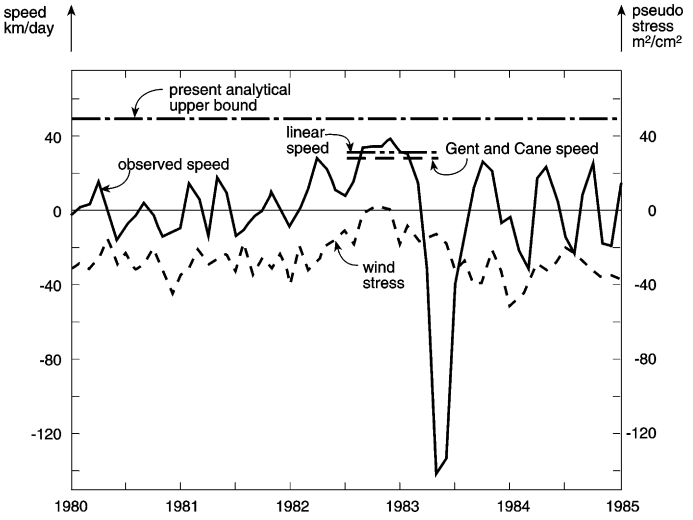

Fig. 7. A comparison of the observed pool's drift (solid line) to the theoretically predicted speed (dashed dotted line) and earlier predictions by the Gent and Cane model (long broken line) and the linear equatorial models (dashed double-dotted line). All are given in km d^{-1}. The pseudo stress (in $m^2\ s^{-2}$) [which was averaged from COADS over a rectangular area extending from 170°E to 160°W (15° east and west of the pool's head mean position) and 4°S to 4°N] is also shown (short broken line). Note that the wind averaged in the above manner diminished completely during the 1982 El Nino, and that, during this year, the observed speed was about 25% lower than the new theoretical prediction and 10% higher than the values given by both Gent and Cane's model and the linear models. The observed position was averaged from 4°N to 4°S. [Aside from our newly computed upper bound, all values are reproduced from the unfiltered data of Picaut and Delcroix (1995) and Picaut et al. (1996)].

chosen values ($\rho_{\text{pool}} \approx 1.022\ \text{g cm}^{-3}$; $\rho_{\text{intermed}} \approx 1.023\ \text{g cm}^{-3}$, $H_1 \approx 150$ m; $H_2 \approx 80$ m). The choice of this new second set of values is just as reasonable as the first one. (Note, however, that, as before, we can choose only those values that are within the model's validity regime.) Using our solution (6.14), (6.9), (6.6) and (6.15) we find a new pool thickness H of about 50 m, a density difference $\Delta\rho_2$ of $0.0032\ \text{g cm}^{-3}$, a speed under the pool U_2 of $1.21\ \text{m s}^{-1}$ and a migration speed of $0.65\ \text{m s}^{-1}$ or $56\ \text{km d}^{-1}$. We see that the newly computed values are not that different from the previous values. Nevertheless, because of the solution third power dependency [e.g., (6.14)], it would be misleading to say that all chosen values would give very similar results. Another sensitivity that should be pointed out here is that if one chooses a range of longitudes and latitudes different than those mentioned in the caption of Fig. 7 then one can find wind averages that do not simply go to zero during the 1982–83 or 1997–98 El Nino. Rather, they may be weak easterlies or even fairly strong westerlies.

7.4. Relationship of predicted speed to the observed speed

We just saw that our nonlinear speed is roughly 25% greater than the observed speed. This can be a result of the model weaknesses or a result of the way that the data

have been handled (or both). We shall first discuss the modeling aspects that can lead to such a difference. As already alluded to, it is possible that the difference is due to the absence of induced motions below the intermediate layer in our model. These motions may exert additional form-drag on the pool and slow it down. Another possibility is that the difference is due to the fact that our model is inviscid and does not include breaking waves. As in the classical two-layer intrusion (Benjamin, 1968), one would expect that, in reality, there would be some sort of breaking waves on the interfaces. These waves cause dissipation and, hence, prevent the Bernoulli from being conserved in the manner that we employed. Due to the reduction of energy, a reduction in the propagation speed is also expected to take place. A third possibility is that there is some recirculation (neglected in our computations), which, as mentioned earlier, slows the pool's propagation down.

An equally reasonable possibility (unrelated to the model) is that the actual migration speed along the equator is greater than the quoted observed values because of the averaging (over a band bounded by 4°N and 4°S) that the observational analysis (i.e., the solid line in Fig. 7) contains. As pointed out earlier, the pool is expected to behave like a forever-thinning tongue with the nose along the equator moving faster than off-equatorial regions. That is to say, in a similar fashion to the propagation of gravity currents along a solid wall on an f-plane, the thickness of the advancing current decreases as one moves away from the equator (wall) until it ultimately vanishes several Rossby radii away. Since the forward speed is proportional to the thickness, this implies that the propagation rate also decreases away from the equator suggesting that the averaging "hides" high propagation rates along the equator.

The importance of such averaging can be easily demonstrated using linear interpolation. From Fig. 1 we see that the pool extends roughly to 8°N and 8°S. Taking into account that the migration speed reduces to zero at these latitudes, and that the averaging was done from 4°N to 4°S, we find (by linear interpolation) that the averaging gives a value that is about 25% less than the maximum speed along the equator. This is roughly the same as the difference between our upper bound and the quoted values for the observed drift, indicating that there may not be any difference at all between our predicted speed and the observed speed along the equator.

A similar comparison of the model to data can be made with the 1997 El Nino but, unfortunately, as of this writing, this El Nino has been only partially analyzed. A simple comparison can, nevertheless, be made. To do so we first note that the FSU tropical Pacific wind stress analysis (Center for Ocean-Atmospheric Prediction Studies, 1998), averaged over a rectangle bounded by 160°E–170°W and 4°N–4°S, shows that during March, April and May of 1997 the winds almost completely relaxed as required by our model. Second, we can see from the SST analysis presented by BMRC (Bureau of Meteorology Research Centre, 1996) that, for the same period, the position of the 28°C isotherm (averaged from 2°N to 2°S) propagated eastward at an average rate of 40–60 km d^{-1}. As pointed out earlier regarding the 1982 El Nino, this propagation rate is roughly equal to our calculated upper bound.

A comment should also be made regarding the observed speed under the pool. According to Kuroda and McPhaden (1993), the water immediately under the pool drifts westward at roughly the same speed as the pool's eastward migration

[10–20 cm s^{-1}, see (their) Fig. 7c], in agreement with our general scenario of an eastward moving pool and a compensating westward (intermediate water) flow immediately underneath. This agreement between the theory and the observations is important, as such westward motions under the pool cannot be explained by a simple Kelvin wave.

Finally, an additional comment should be made regarding our use of the no-recirculation assumption. As we saw, without recirculation, the zonal eastward pressure gradient is balanced by form-drag exerted on the pool by the intermediate water that is diving underneath the eastward propagating pool. With anticyclonic recirculation, part of this zonal pressure gradient would be balanced by the equatorward meridional flow near the "nose" of the pool and, consequently, the pressure gradient available to drive the pool forward would be reduced. This is consistent with the familiar idea that moving fronts are generated and maintained by *ageostrophic* and not geostrophic motions (see, e.g., Hoskins and Bretherton, 1972; Nof, 1979). It means that the recirculation would slow the pool's migration rate down so that its neglect for the purpose of computing our upper bound limit is certainly adequate.

8. Summary

Before listing our conclusions it is appropriate to mention again that, although our two-and-a-half-layer model (Fig. 3) is fully nonlinear, it neglects the effects of energy loss and friction. It also neglects the drag that is usually exerted on the pool by the trade winds, implying that the model results are applicable only to those situations when the winds completely relax (e.g., the 1982 and 1997 El Ninos). The results can be summarized as follows:

1. By considering a control volume that extends a few deformation radii away from the pool's nose in the east–west direction and an infinitesimal distance ε in the north–south direction (Fig. 3), considering the corresponding flow-force, energy, mass, and potential vorticity conservation, assuming that there is no recirculation, and then taking the limit as $\varepsilon \to 0$, we show that an infinitesimal band of water in the immediate vicinity of the equator moves steadily eastward.
2. When the above limit is taken, all the terms involving the Coriolis parameter drop out of the problem demonstrating that, under such conditions, a narrow band in the immediate vicinity of the equator is not directly affected by the earth's rotation. This essentially results from the symmetry of the problem (relative to the equator), which implies no cross-equatorial flow within the head of the pool and no east–west Coriolis force. The above limit gives an upper bound for the migration speed because the thickness of the pool decreases gradually away from the equator [implying that the forward propagation rate (which is proportional to the thickness) also decreases away from the equator].
3. For a given pool's thickness (and intermediate layer thickness ahead of the pool) and a given density difference between the pool and the intermediate water below, there is one propagation rate (Figs. 5 and 6), one thickness under the pool and one

density difference ratio (i.e., one ratio of the density difference between the pool and the intermediate water and the density difference between the intermediate water and the deep water underneath).

4. The calculated upper bound for the eastward migration of the pool's nose is $[2g(\Delta\rho_1/\rho)H]^{1/2}\,(H_2/H_1)$, where $\Delta\rho_1$ is the density difference between the pool and the water underneath and H, H_1 and H_2 are the pool thickness, the intermediate water thickness ahead of the pool and the intermediate water thickness under the pool. The above formula is simple to use but it does not contain all the information that the model provides. Specifically, according to Eq. (6.14) there is a particular ratio between H and H_1 for any given pool so that, from a theoretical point of view, the migration speed should be written in terms of only *three* variables, e.g., $C = [2g(\Delta\rho_1/\rho)H_1]^{1/2}\,(1 - H_2/H_1)^{3/2}$.

There are three aspects of the model that agree with the observations. First, it turns out that the combined pool and intermediate layer depth under the pool ($H + H_2$) is always smaller than the intermediate layer depth ahead of the pool, H_1 (Fig. 6), so that the modeled interface rises under the pool. This is supported by Kuroda and McPhaden's (1993) observation of the pool (see Fig. 2) even though the winds did not completely collapse during the year that the observations were made (1990). Furthermore, all the measured density differences and depths are also in good agreement with the theoretical predictions. Apparently, the drag induced by the trade winds prevented a continuous free eastward movement but did not alter the density field significantly. Second, and most important, a comparison of the predicted and observed migration speeds during the 1982 El Nino (Fig. 7) shows that our predicted nonlinear upper bound is about 25% higher than the averaged observed speed, and about 40% higher than the speed predicted by both the Gent and Cane model and the earlier linear model. The difference between our upper bound and the observed values is either due to our neglect of friction, breaking waves and recirculation (which would reduce the computed speed) or due to the averaging of the pools observed speed over an 8° band (that "hides" the actual speed along the equator, which is expected to be greater than the off-equatorial speed) or both. Third, a comparison between the modeled speed under the pool to the observed speed under the pool shows that, as required, both speeds reverse direction with depth (i.e., both display a westward speed underneath the pool).

As of this writing the analysis of the 1997 El Nino has not been completed to a degree that a detailed satisfactory comparison to the data can be made. A simple comparison is nevertheless possible and gives very reasonable values.

Notation

B	Bernoulli invariant
C	pool migration speed
C_p	water heat capacity
g'_1, g'_2	reduced gravity ($= \Delta\rho_1/\rho)g, (\Delta\rho_2/\rho)g$)

h	pool thickness
h_2	thickness of the intermediate layer
H	upstream pool thickness along the equator
H_1	intermediate water thickness ahead of the pool (along the equator)
H_2	intermediate water thickness above the pool (along the equator)
p	pressure
P	potential vorticity
Q	anomalous heat flux to the atmosphere
S	entire area of control box
S_p	fractional area of the box occupied by the pool
t	time
T	temperature
u, v	velocities in the moving Cartesian coordinates
U_2	intermediate layer speed above the pool (along the equator)
x_s, y_s, t_s	scaled variables associated with a stationary [but rotating ($\beta \neq 0$)] coordinate system
y_i	latitude from which the parcel originated
z	height
β	variation of the Coriolis parameter with latitude
ε	half the meridional extent of the control volume
ρ	reference density
$\Delta\rho_1$	density difference between the pool and the intermediate layer
$\Delta\rho_2$	density difference between the intermediate and deep water
ϕ_p	boundary of the pool within the control box
ψ, ψ_2	usual streamfunction of the pool and intermediate water in the moving coordinates system
τ	wind stress
v	viscosity

Acknowledgements

This study was supported by the National Science Foundation (NSF) under grants OCE 9102025 and OCE 9503816, National Aeronautics and Space Administration (NASA) grants NAGW-4883 and NAG5-4813, and Office of Naval Research (ONR) grant N00014-96-1-0541. Conversations with A. Clarke and correspondence with M. McPhaden and W. Kessler were very helpful. We thank T. Delcroix for providing us with his unfiltered data for the observations and numerical values shown in Fig. 7.

References

Benjamin, T.B., 1968. Gravity currents and related phenomena. Journal of Fluid Mechanics 31, 209–248.

Bjerknes, J., 1969. Atmospheric teleconnections from the equatorial Pacific. Monthly Weather Review 97, 163–172.

Bjerknes, J., 1972. Large-scale atmospheric response to the 1964–65 Pacific equatorial warming. Journal of Physical Oceanography 2, 212–217.

Bureau of Meteorology Research Centre, 1996. BMRC Climate Group Experimental Results, Commonwealth Bureau of Meteorology, Australia, http://www.bom.gov.au/bmrc/mrlr/SST_anals/.

Cane, M.A., Patton, R.J., 1984. A numerical model for low-frequency equatorial dynamics. Journal of Physical Oceanography 14, 1853–1863.

Cane, M.A., Zebiak, S.E., 1985. A theory on El nino and the South Oscillation. Science 228, 1985–1987.

Center for Ocean-Atmospheric Prediction Studies, 1998. FSU/COAPS Tropical Pacific Ocean Pseudostress Analyses, Center for Ocean-Atmospheric Prediction Studies, Florida State University, http://www.coaps.fsu.edu/WOCE/html/pacwinds.htm.

Delcroix, T., Eldin, G., Radenac, M.-H., Toole, J.M., Firing, E., 1992. Variations of the western equatorial Pacific Ocean, 1986-1988. Journal of Geophysical Research 96, 3249–3262.

Delcroix, T., Picaut, J., 1998. Zonal displacement of the western equatorial Pacific fresh pool. Journal of Geophysical Research 103, 1087–1098.

Delecluse, P., Madec, G., Imbard, M., Lévy, C., 1993. OPA Version 7 Ocean General Circulation model reference manual. LODYC, France, Internal Rep. 93/05, 111 pp.

Firing, E., Lukas, R., Sadler, J., Wyrtki, K., 1983. Equatorial undercurrent disappears during 1982–1983 El Nino. Science 222, 1121–1123.

Gill, A.E., 1982. Atmospheric-Ocean Dynamics, Academic Press, 662 pp.

Griffiths, R.W., 1986. Gravity currents in rotating systems. Annual Review of Fluid Mechanics 18, 59–89.

Halpern, D., 1987. Observations of annual and El Nino flow variations at 0°, 110°W and 0°, 95°W during 1980–1985. Journal of Geophysical Research 92, 8197–8212.

Hoskins, B.J., Bretherton, F.P., 1972. Atmospheric frontogenesis models. Mathematical formulation and solution. Journal of Atmospheric Science 29, 11–27.

Kubokawa, A., Hanawa, K., 1984a. A theory of semigeostrophic gravity waves and its application to the intrusion of a density current along a coast. Part I. Semigeostrophic gravity waves. Journal of Oceanographic Society of Japan 40, 247–259.

Kubokawa, A., Hanawa, K., 1984b. A theory of semigeostrophic gravity waves and its application to the intrusion of a density current along a coast. Part II. Intrusion of a density current along a coast in a rotating fluid. Journal of Oceanographic Society of Japan 40, 260–270.

Kuroda, Y., McPhaden, M.J., 1993. Variability in the Western Equatorial Pacific Ocean during Japanese Pacific Climate study cruises in 1989 and 1990. Journal of Geophysical Research 98, 4747–4759.

Long, R., 1955. Some aspects of the flow of stratified fluids III. Continuous density gradients. Tellus 3, 341–357.

Maes, C., Delecluse, P., 1998. Impact of westerly wind bursts on the warm pool of the TOGA-COARE domain in an OCGM. Climate Dynamics 14, 55–70.

Myers, P., Fanning, A., Weaver, A., 1996. JEBAR, bottom pressure torque, and Gulf Stream separation. Journal of Physical Oceanography 26, 671–683.

McPhaden, M.J., Freitag, H.P., Hayes, S.P., Taft, B.A., Chen, Z., Wyrtki, K., 1988. The response of the equatorial Pacific Ocean to a westernly wind burst in May 1986. Journal of Geophysical Research 93, 10589–10603.

McPhaden, M.J., Picaut, J., 1990. El Nino-Southern Oscillation displacements of the western equatorial Pacific warm pool. Science 250, 1385–1388.

Murtugudde, R.R., Seager, R., Busalacchi, A.J., 1996. Simulation of the tropical oceans with an ocean GCM coupled to an atmospheric mixed-layer model. Journal of Climate 9, 1795–1815.

Nof, D., 1979. Generation of fronts by mixing and mutual intrusion. Journal of Physical Oceanography 9, 298–310.

Nof, D., 1987. Penetrating outflows and the dam-breaking problem. Journal of Marine Research 45, 557–577.

Picaut, J., Delcroix, T., 1995. Equatorial wave sequence associated with warm pool displacements during the 1986–1989 El Nino-La Nina. Journal of Geophysical Research 100, 18393–18408.

Picaut, J., Ioualalen, M., Menkes, C., Delcroix, T., McPhaden, M.C., 1996. Mechanism of the zonal displacements of the Pacific warm pool: implications for ENSO. Science 274, 1486–1489.

Picaut, J., Masia, F., du Penhoat, Y., 1997. An advective-reflective conceptual model for the oscillatory nature of the ENSO. Science 277, 663–666.

Roemmich, D., Morris, M., Young, W.R., Donguy, J.R., 1994. Fresh equatorial jets. Journal of Physical Oceanography 24, 540–558.

Simpson, J.E., 1987. Gravity Currents in the Environment and the Laboratory. Wiley, New York, 244 pp.

Stern, M., 1980. Geostrophic fronts, bores, breaking and blocking waves. Journal of Fluid Mechanics 99, 687–703.

Stern, M., Whitehead, J.A., Hua, B.L., 1982. The intrusion of a density current along the coast of a rotating fluid. Journal of Fluid Mechanics 123, 237–265.

Vialard, J., Delecluse, P., 1998a. An OGCM study for the TOGA decade, Part I: role of salanity in the physics of the western Pacific fresh pool. Journal of Physical Oceanography 28, 1071–1088.

Vialard, J., Delecluse, P., 1998b. An OGCM study for the TOGA decade, Part II: intermediate layer formation and variability. Journal of Physical Oceanography 28, 1089–1106.

Von Karman, T., 1940. The engineer grapples with nonlinear problems. Bulletin of American Mathematical Society 46, 615.